# Enhancement of organophosphate degradation by electroactive pyrrole and imidazole copolymers

*Bruna M. Hryniewicz,[a] Franciele Wolfart,[b] Pedro Gómez-Romero,[c] Elisa Orth*[d] and Marcio Vidotti *[a]**

[a]Grupo de Pesquisa em Macromoléculas e Interfaces, Departamento de Química, Universidade Federal do Paraná, CP 19032, 81531-980, Curitiba, PR, Brazil.

[b]Instituto Federal Farroupilha - Campus São Borja, Rua Otaviano Castilho Mendes, 355, Betim, CEP 97670-000, São Borja - RS, Brazil

[d]Catalan Institute of Nanoscience and Nanotechnology (ICN2), CSIC and The Barcelona Institute of Science and Technology, Campus UAB, Bellaterra, 08193 Barcelona, Spain

[d] Grupo de Catálise e Cinética, Departamento de Química, Universidade Federal do Paraná, CP 19032, 81531-980 Curitiba, PR, Brazil

KEYWORDS:

**Abstract**

Many chemical warfare agents and agrochemicals are composed by organophosphates, that present high toxicity and difficult spontaneous degradation. Amongst the different catalysts for degradation of these compounds, heterogeneous systems stand out since they provide easy recovery of the catalyst. On the other hand, the limited diffusion of the substrate to the active sites decreases the rate of the reactions when compared to homogeneous catalysis. To reach a good efficiency in the dephosphorylation, we created heterogeneous catalysts that can enhance the degradation by different effects. Copolymers based on imidazole and pyrrole were synthesized by chemical polymerization and both catalytic activity of imidazole and electroactivity of polypyrrole were evaluated. The results showed that the copolymers with high imidazole contents presented good catalytic activity. Furthermore, spectroelectrochemical studies evidenced that the rate constant changes with the applied potential, indicating different reaction mechanisms with the material in the oxidized and neutral states. In summary, the copolymers synthesized are good candidates as detoxifying agents and a new perspective allying conducting polymers with chemical catalysts was explored. This cooperative effect should be considered in future works concerning the search for new materials to monitor and eliminate organophosphates, as well in the design of new artificial enzymes.

## 1. Introduction

Organophosphates (OP) are widely used as pesticides throughout the world due to their high efficiency [1] and economic feasibility [2]. Many of these compounds also constitute chemical warfare [3,4] and act in the central nervous system of humans and insects, inhibiting the acetylcholinesterase enzyme [5,6]. This inhibition prevents the hydrolysis of acetylcholine, which then accumulates in cholinergic receptors, causing excess stimulation of the nerve fiber [5]. Because OPs show benefits in controlling pests [7] there is no perspective of banning their application in agriculture, but the inappropriate use of these compounds can cause several health issues [8,9] and, once the individual is intoxicated, the treatment may not be fast enough to save the life of the patient or avoid permanent damages [4].

Another concern about OPs is the presence of highly stable P-O bonds in their structures that leads to bioaccumulation, which means that they can be active in the environment for long periods [10,11]. For example, Paraoxon has an estimated life-time of 516 million years for spontaneous degradation [12], highlighting the importance to develop catalysts that can accelerate the degradation process. Currently, many approaches have been used in OPs degradation [1], such as homogeneous and heterogeneous catalysis [12–15], photolysis [16–18] and biodegradation [8]. Among different catalysts, materials based on imidazole (IMZ) and its derivatives have shown excellent behavior in the detoxification of OPs [19], biomimicking the histidine imidazole in the protein phosphorylation [20,21]. The histidine imidazole in protein enzymes is the most versatile catalytic group, with a pKa near 7, it can act as an acid, base or nucleophilic catalyst [22,23]. Several studies confirmed that cleavage of phosphate esters can be catalyzed by the presence of IMZ, with catalytic increments around $10^5$-fold [10,14,22], combined with the advantages of complete regeneration of

the initial catalyst and formation of less toxic compounds. Considering that the recovery and subsequent reuse of catalysts in heterogeneous systems is easier than from homogeneous analogues, different approaches have been reported to anchor IMZ and its derivatives in lattices such as those formed by organic polymers. As an example, it has been observed that the decomposition rate constant obtained with IMZ immobilized in polymeric frameworks [24] was greater than those of soluble IMZ derivatives. Accordingly, a biocatalyst based on IMZ anchored on gum arabic [25] demonstrated high catalytic activity ($10^5$-fold) and recyclability in dephosphorylation reactions. Recently, it has been reported that a heterogeneous system based on an IMZ-graphene composite promoted efficient OP destruction with impressive rate enhancements (around $10^6$-fold) [12]. This improvement is very significant when compared to other heterogeneous catalysts found in the literature, such as copper-containing amyloids, which produced catalytic enhancements of about $10^3$-fold [13]; nanocapsules of enzyme-mimic molecular imprinted polymers, with a rate increment of 415-fold in comparison with self-hydrolysis, and requiring a treatment in NaOH and aqueous $Zn^{2+}$ solution to reuse the catalyst [11]; porous materials based on chromium(III) terephthalate metal organic frameworks MIL-101(Cr) and their complexes with dialkylaminopyridines (140-fold faster than spontaneous hydrolysis) [26]; and titania-based mesoporous film, with catalytic activity 27% higher than background hydrolysis [27].

In a previous study, we reported the electrochemical synthesis of an imidazole-modified polypyrrole (PPy) system, which was made possible by the structural similarity between IMZ and pyrrole (Py) [28]. XPS, Raman spectra and kinetic studies proved that the material obtained was a copolymer. This product, in which IMZ appears to improve pseudocapacitive properties, was shown to be promising as a supercapacitor

electrode. Herein, we report the chemical synthesis of Py and IMZ copolymers to be used as heterogeneous catalysts for OP degradation. In this case, PPy was not only intended to act as a matrix to anchor IMZ molecules, but its electrochemical properties could also influence the catalytic efficiency.

In this work, the syntheses were followed by UV-visible spectroscopy and the products were characterized by X-ray photoelectron spectroscopy (XPS). The catalytic activity of the samples was evaluated in the dephosphorylation reaction of the triester diethyl 2,4-dinitrophenylphosphate (DEDNPP), and the influence of the PPy oxidation state in the chemical catalysis was studied by an innovative spectroelectrochemical methodology. Results demonstrate the great potentiality of the copolymers for DEDNPP degradation, with the possibility of rate enhancement by changing the redox state of PPy, which could promote a higher exposure of IMZ catalytic sites.

## 2. Experimental

### 2.1. Materials

All solutions were prepared with ultrapure water (Milli-Q, R = 18.2 MΩ·cm). Pyrrole (Py) monomer (97%, Aldrich) was purified by distillation and purged by bubbling with $N_2$. Imidazole (IMZ), sodium dodecylbenzenesulfonate (DBS), sodium acetate, potassium phosphate and ammonium persulfate (APS), all purchased from Aldrich, were used as acquired. Diethyl 2,4-dinitrophenylphosphate (DEDNPP) was synthesized as previously described [10].

### 2.2. Chemical synthesis of copolymers

Freshly distilled Py was added to acetate buffer (10 mmol $L^{-1}$, pH 5) containing DBS (1 mmol·$L^{-1}$) and IMZ. The concentrations of Py and IMZ used in the syntheses of the different samples are shown in Table 1.

Table 1. Concentrations of Py and IMZ used in the chemical syntheses.

| Sample | Py:IMZ proportion | [Py] / mmol $L^{-1}$ | [IMZ] / mmol $L^{-1}$ |
|---|---|---|---|
| p(Py:IMZ-0) | 100:0 | 26.40 | 0.00 |
| p(Py:IMZ-10) | 90:10 | 23.76 | 2.64 |
| p(Py:IMZ-25) | 75:25 | 19.80 | 6.60 |
| p(Py:IMZ-40) | 60:40 | 15.84 | 10.56 |
| p(Py:IMZ-50) | 50:50 | 13.20 | 13.20 |
| p(Py:IMZ-60) | 40: 60 | 10.56 | 15.84 |

The polymerization was initiated by adding APS to the reaction medium. The reaction mixture was kept stirring for 24 h at 25 ºC. The molar ratio of [APS]/[Py] was 0.14 for the kinetics studies (to prevent polymer precipitation) and 1.3 for all other measurements. The polymerization reaction was monitored at 25 ºC by UV-Vis spectroscopy (Spectrophotometer UV-Vis Agilent 8453) in a 3-mL quartz cuvette. Kinetic profiles (absorbance *versus* time) were obtained at 840 nm (characteristic band of PPy formation) for 6 h and fitted adopting a non-linear model for first-order reactions ($R^2$ > 0.99). The p(Py:IMZ_0), p(Py:IMZ_25) and p(Py:IMZ_50) samples were characterized by X-ray photoelectron spectroscopy (XPS) on a SPECS Germany PHOIBOS 150 hemispherical energy analyzer with a resolution of 0.2 eV. FTIR spectra of the powders were acquired in KBr pellets using a Bruker Vertex 70 spectrometer in transmission mode with 4-$cm^{-1}$ resolution.

2.3. Catalytic activity

The catalytic activity of the composites towards DEDNPP degradation was evaluated by monitoring the dephosphorylation reaction by UV-Vis spectroscopy in the presence of the different copolymers. The studies were performed using 5 mg of the samples dispersed in 5 mL of phosphate buffer (10 mmol $L^{-1}$, pH 8.0), and the reaction was started by adding DEDNPP at the final concentration of 0.091 mmol $L^{-1}$. The reaction mixture was kept stirring for 6 h and the spectra were acquired in quartz cuvettes at intervals of 50 min. Dephosphorylation was followed by the appearance of the 2,4-dinitrophenolate (DNP) band measured at 360 nm, and the pseudo first-order rate constants ($k_{obs}$) were obtained using the initial rate methodology.

2.4. Electrochemical influence in the dephosphorylation reaction

Electrochemical measurements were performed to understand the influence of the PPy oxidation state in the dephosphorylation reaction. The experiments employed Autolab PGSTAT 204 and Ivium Stat.XRE potentiostats, Pt foil as counter electrode and $Ag/AgCl/Cl^-_{sat}$ as reference electrode. Indium tin oxide (ITO) electrodes modified with the samples were used as working electrodes. For preparation of these electrodes, the p(Py:IMZ-0) and p(Py:IMZ-50) samples were first dispersed in acetone containing 5% (m/v) of Nafion®. Then, an aliquot of the dispersion was drop-casted onto the ITO surface and dried under vacuum for 24 h before the electrochemical tests.

Cyclic voltammetry (CV) and electrochemical impedance spectroscopy (EIS) tests were employed to evaluate whether the materials presented electrocatalytic activity. The experiments were carried out in 1 mol $L^{-1}$ $Na_2SO_4$ in the absence and in the presence of 0.091 mmol $L^{-1}$ DEDNPP. EIS was performed using three different d.c. potentials: 0.6 V, -0.45 V and open circuit potential (ocp), with an a.c. potential of 10 mV and frequencies ranging from 10 kHz to 10 mHz. *In-situ* UV-Vis spectroelectrochemical experiments were then carried out to evaluate the influence of

the applied potential in the dephosphorylation reaction. These analyses were performed in a quartz cuvette containing phosphate buffer and 0.091 mmol $L^{-1}$ of DEDNPP using modified ITO as working electrode, Pt foil as counter electrode and Ag/AgCl as reference electrode, with the application of 0.6 V, -0.45 V and ocp for 110 min.

## 3. Results and Discussion

### 3.1. Synthesis and characterization of the catalysts

The syntheses of the different samples were followed by UV-Vis spectroscopy. As can be seen in Fig. S1, the formation of PPy is characterized by the appearance of a band at 445 nm, assigned to the π-π* transition and a broad band at 840 nm, related to the bipolaronic state [29]. The intensity of the band at 840 nm was monitored throughout the reaction time to provide the kinetic data for the polymerization in the presence of IMZ, as can be seen in Fig. 1 (a). The rate constant ($k_{PPy}$) for the different samples was obtained by fitting the experimental data using a model for first order reactions and the results are shown in Fig. 1 (b).

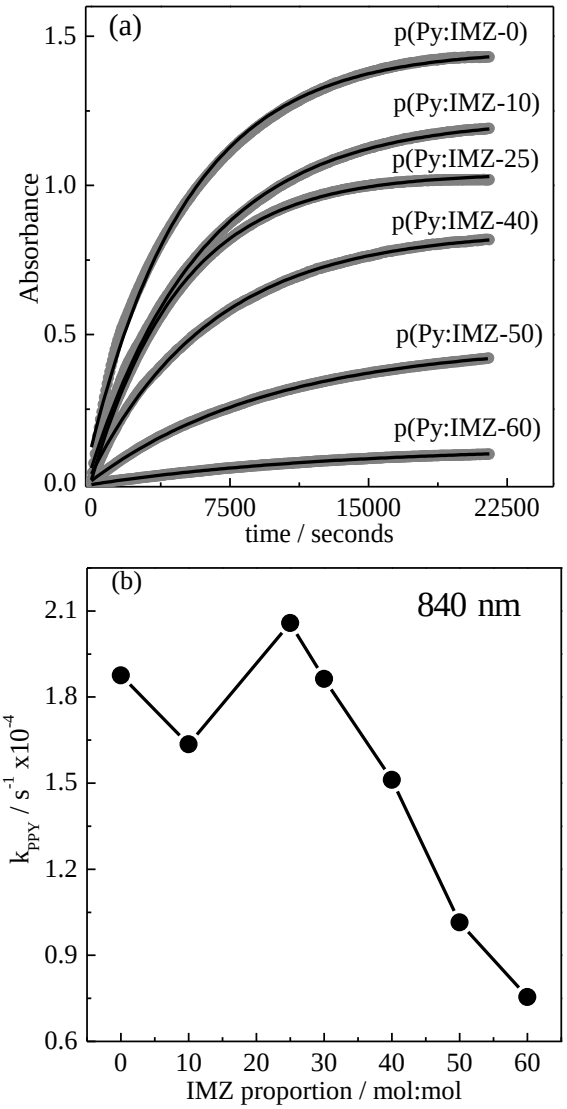


Fig. 1. (a) Experimental kinetic profile of copolymer growth in different proportions of imidazole; the black line is the fitted plot. (b) Polymerization rate constants for different Py:IMZ proportions, obtained from the fit showed in (a).

It is possible to observe a general behavior that with higher IMZ content, the rate constant decreases, in which case IMZ could be acting as an inhibitor for Py polymerization. This behavior was observed earlier for poly(3,4-ethyelenedioxythiophene) (PEDOT) polymerization in the presence of IMZ [30], and also for PPy-IMZ electrochemically synthesized [31]. The inhibitor nature of IMZ could be attributed to the pH increase that results from the presence of the amine in the

solution, since the polymerization of PPy is hampered in basic media. Also, the structural similarity between IMZ and Py could result in a competition during the polymerization, which eventually leads to IMZ trapped on the final product, and results in the copolymer.

The formation of the copolymers was confirmed by XPS measurements, as can be seen in Fig. 2.

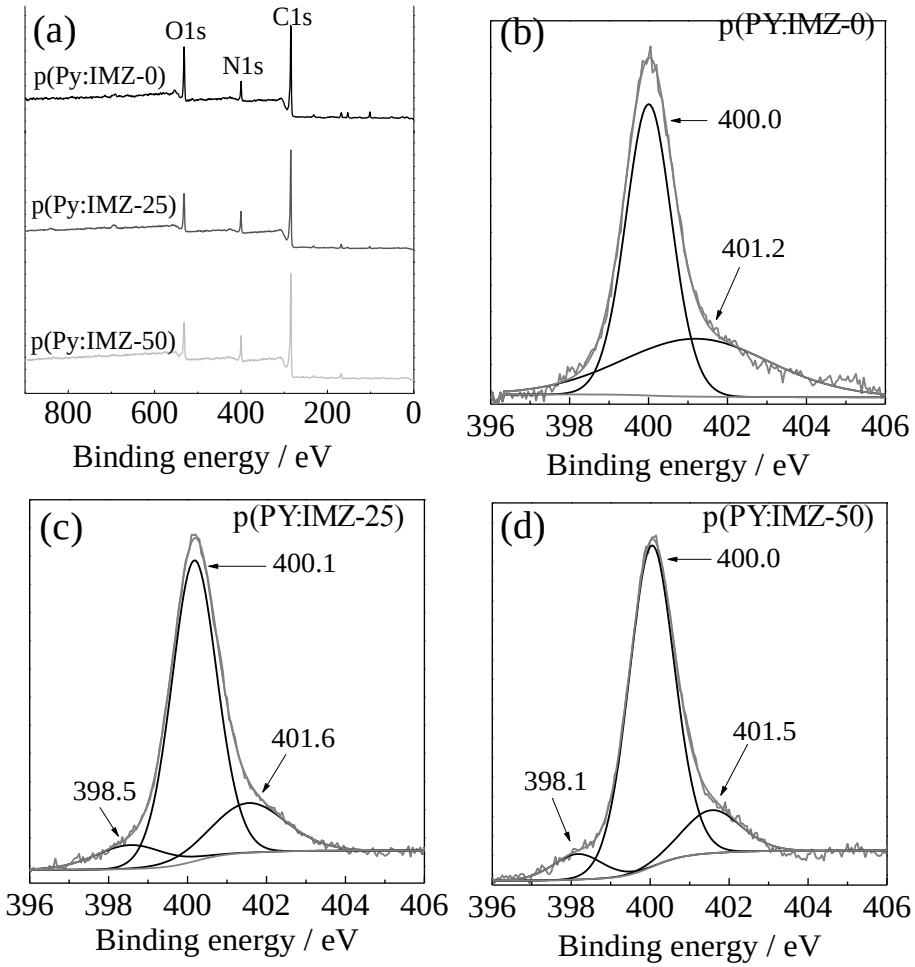


Fig. 2. (a) XPS spectra of a wide region spectra for different copolymers; (b)-(d): the N1s peak region for p(Py:IMZ-0) (b); p(Py:IMZ-25) (c) and p(Py:IMZ-50) (d) samples.

Fig. 2(a) shows the wide region of p(Py:IMZ-0), p(Py: IMZ-25) and p(Py:IMZ-50), presenting the characteristic peaks of N1s (~400.5 eV), C1s (~284.5 eV) and O1s

(~532.8 eV). The features in the O1s region can be attributed to the surface oxidation of PPy [32] and the presence of DBS as dopant in the polymeric chain [33]. The N1s and C1s peaks are from the PPy backbone; however, the intensity of the N1s increases in the presence of IMZ (Table 2). The deconvolution of the N1s signal revealed two and three components, respectively, in p(Py:IMZ-0) and in the two IMZ-containing samples (Fig. 2(b-d)). The N1s components at 398.4, 400.0 and 401.5 ($\pm$0.2) eV are attributed to quinoid imine (C=N), benzenoid amine (-NH) and protonated benzenoid amine ($-NH^+$), respectively [32,34]. Interestingly, the quinoid imine component at 398.4 eV only appears in samples obtained in the presence of IMZ, suggesting its insertion in the PPy chain and supporting the formation of the copolymer. In addition, the increment in the proportion between quinoid and neutral bonds ((C=N)/(-NH)) and the increase in the nitrogen content of samples obtained in the presence of IMZ suggest that this monomer was properly inserted in the polymeric chain (Table 2).

Table 2. Results obtained by XPS studies.

| **Parameter** | **Sample** | | |
|---|---|---|---|
| | **p(Py:IMZ-0)** | **p(Py:IMZ-25)** | **p(Py:IMZ-50)** |
| **C %** | 79.1 | 81.4 | 79.9 |
| **N %** | 7.5 | 8.7 | 9.5 |
| **O %** | 13.4 | 9.9 | 10.6 |
| **(C=N)/(-NH) %** | 0 | 10.3 | 17.8 |

The formation of the copolymer was also evidenced by FTIR spectra, as shown in Fig. S2. In presence of IMZ bands at 1670 $cm^{-1}$, attributed to C=N bend of IMZ molecules [35,36], and at 926 $cm^{-1}$ [37], associated with the N-H in plane IMZ ring

bend, increases in the copolymers with higher amounts of IMZ. Furthermore, the band at 655 $cm^{-1}$ [37], related to the C-N-C bending in the IMZ ring, increases with higher content of IMZ, supporting its presence in the polymeric matrix.

The copolymers were analyzed by TEM and the images are shown in Fig. S3. Particles are homogeneously distributed, but the morphology of the materials did not change in the presence of IMZ.

### 3.2. Heterogeneous catalysis of DEDNPP

After characterization, the samples were investigated as potential catalysts in the dephosphorylation of DEDNPP, a model substrate employed in OP degradation reactions. In this context, IMZ molecules present in the PPy matrix could attack the phosphorus center of DEDNPP generating a phosphorylated intermediate together with 2,4-dinitrophenolate (DNP). The intermediate then decomposes regenerating the catalyst (Fig 3a) [25,38]. It should be noted that Py is not reactive towards OP as a nucleophile. Dephosphorylation can be evidenced by the decrease in the band at 257 nm, indicating the consumption of DEDNPP, and the appearance of the band at 360 nm, related with the DNP formed during the reaction (Fig. 3b).

The kinetic profile of dephosphorylation was obtained by following the band at 360 nm. The rate constants ($k_{obs}$) were obtained for the different samples (Fig. 3c) by the initial rate method and normalized for the mass of the copolymer. There is a clear increment in $k_{obs}$ for the samples containing IMZ, suggesting the IMZ-insertion in the material. Also, the p(Py:IMZ-50) and p(Py:IMZ-60) samples showed a $5\times10^3$-fold rate increment in comparison to the spontaneous degradation [22]. This increment is higher than that provided by IMZ in homogeneous catalysis ($2\times10^3$-fold) [22] and similar to

other results reported elsewhere [39], suggesting that the PPy-IMZ copolymer obtained by this simple method has a great potential for the degradation of OP.

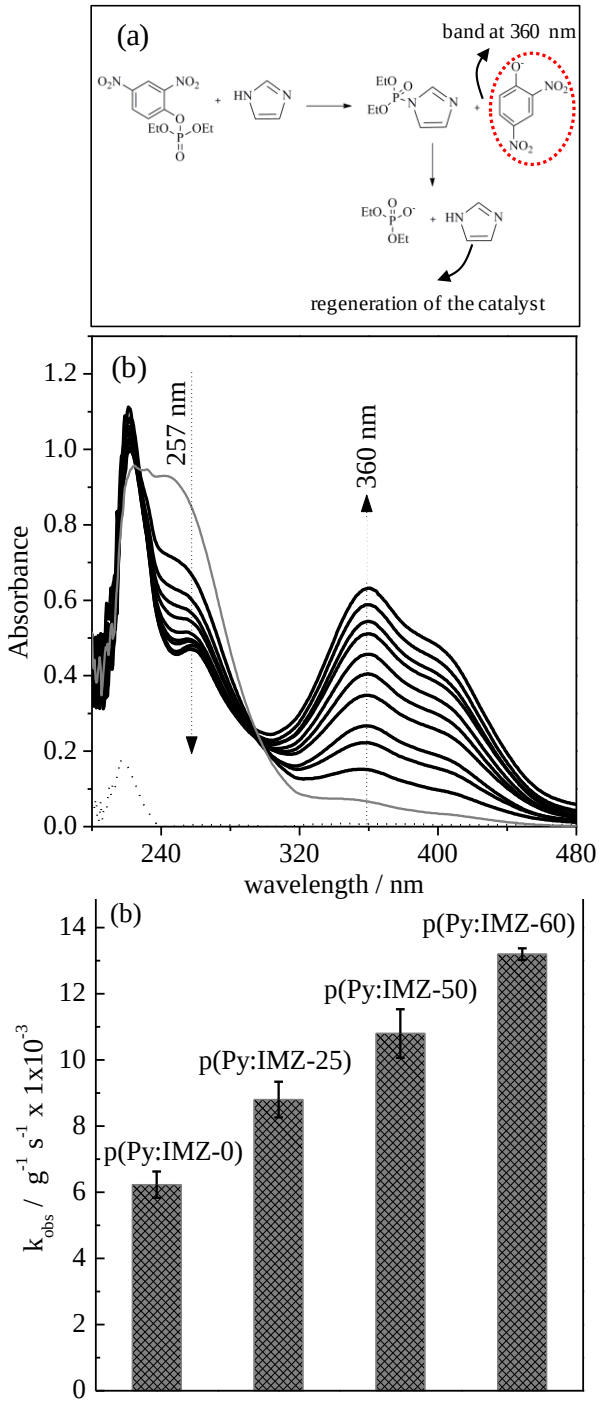


Fig. 3. (a) Mechanism of dephosphorylation in the presence of IMZ. (b) UV-Vis spectra registered in time intervals during the degradation of DEDNPP with p(Py:IMZ-50) as catalyst. (c) Rate constants for the degradation of DEDNPP with different copolymers as catalysts.

The rate increments obtained with the copolymers are significant considering the heterogeneous nature of the catalytic system, which can hamper the diffusion of OP to the IMZ active sites, and the low quantity of IMZ in the copolymer, which is probably lower than the content of Py. In addition, this method allows both recovery and reuse of the catalyst, decreasing the amount of residues after OP destruction.

### 3.3. Spectroelectrochemical study of DEDNPP degradation

The samples containing 0% and 50% of IMZ were deposited on ITO electrodes using Nafion® as a binder agent. The electrodes were cycled at 20 mV $s^{-1}$ in 1 mol $L^{-1}$ $Na_2SO_4$ in the absence and presence of DEDNPP, and the results are shown in Fig. 4 (a) and Fig. 4 (b) for p(Py:IMZ-0) and p(Py:IMZ-50), respectively. Firstly, both electrodes present large capacitive currents and broad redox waves; the p(Py:IMZ-50) modified electrode showed the highest current, as it was also observed earlier for the electrosynthesized material [31]. A decrease in the current in the presence of DEDNPP was also observed in both cases; this behavior indicates that DEDNPP adsorbs at the electrode surface forming an insulating layer and a barrier for the charge transfer processes [40]. As a consequence, the decomposition of DEDNPP is not electrocatalyzed in the potential window studied, since an electrocatalytic process is identified by the appearance of new redox waves in the voltammogram, not verified here. Furthermore, the decrease in the current was more significant in the IMZ-containing samples, corroborating the possible interaction of IMZ with OP that could increase the number of DEDNPP molecules adsorbed on the electrode surface.

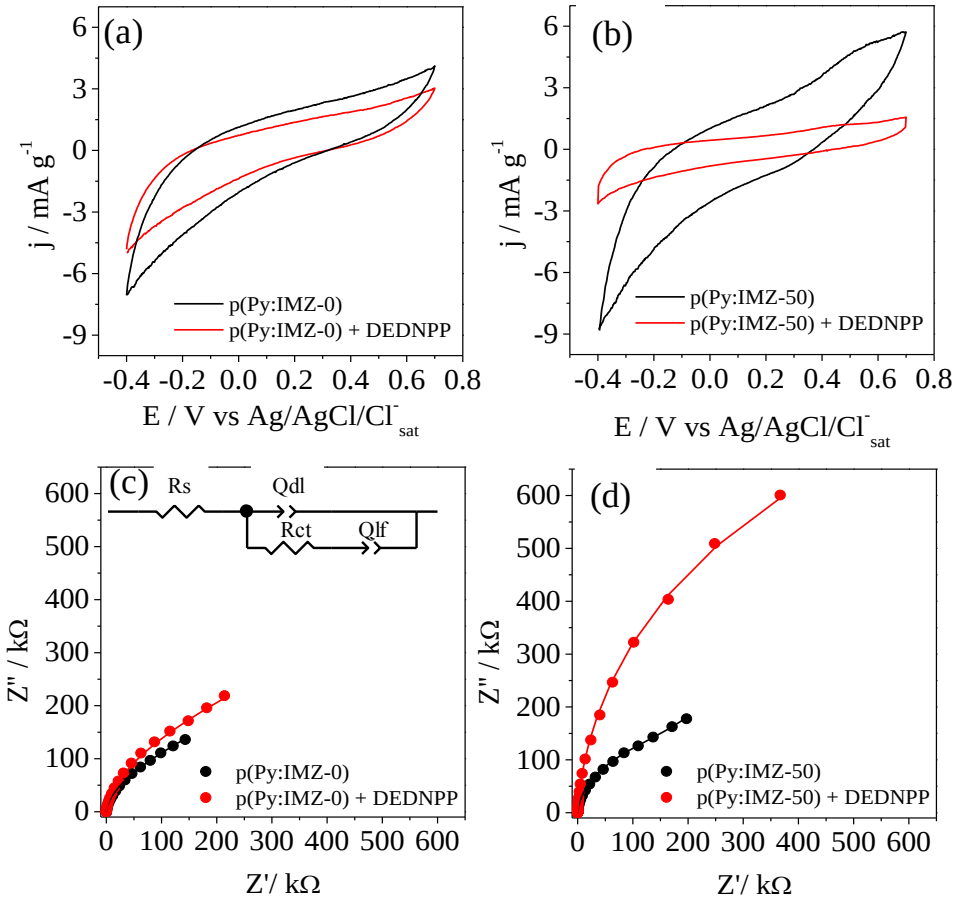


Fig. 4. Cyclic voltammetry of (a) p(Py:IMZ-0) and (b) p(Py:IMZ-50) samples in 1 mol $L^{-1}$ $Na_2SO_4$ in the presence and absence of DEDNPP, scan rate of 20 mV $s^{-1}$. Nyquist plots obtained from EIS data for (c) p(Py:IMZ-0) and (d) p(Py:IMZ-50). The equivalent circuit used to fit the experimental data is inserted on (c).

The samples were also characterized by EIS measurements. The Nyquist plots obtained for p(Py:IMZ-0) and p(Py:IMZ-50) are shown in Fig. 4 (c) and Fig. 4 (d), respectively. The data were fitted using an equivalent circuit commonly employed for conducting polymers [41,42], inserted on Fig. 4 (c). This circuit is composed by a series resistance (*Rs*), which is related with the resistance of the electrode, electrolyte, connections and the deposited material, a charge transfer resistance (*Rct*), assigned to the resistance of the charge transfer processes at the electrode surface, a constant phase

element accounting for the double layer capacitance (*Qdl*) and a constant phase element assigned to the low frequency capacitance (*Qlf*), which is related to the ion intercalation process in the polymer matrix to guarantee its electroneutrality. The parameters calculated from EIS data are shown in Table 3.

Table 3. Parameters obtained through fitting of the EIS data using the equivalent circuit inserted on Fig. 4 (c).

| **Sample** | **Rs** | **Rct / kΩ** | **Qdl / µF $s^{n-1}$** | **Qlf / µF $s^{n-1}$** |
|---|---|---|---|---|
| p(Py:IMZ-0) | 24.0 | 19.8 | 7.4 | 8.5 |
| p(Py:IMZ-0) + DEDNPP | 23.0 | 36.9 | 7.5 | 6.1 |
| p(Py:IMZ-50) | 31.7 | 174.9 | 9.5 | 16.5 |
| p(Py:IMZ-50) + DEDNPP | 33.6 | 1310.5 | 8.2 | 17.5 |

The differences observed in the *Rs* value cannot be discussed in terms of polymeric conductivity since *Rs* can be affected by differences in the thickness of Nafion® layer and in the connections of the electrodes. The most interesting circuit element in this work is the *Rct*, which is directly related to the facility to transfer the charges at the electrode interface. An electrocatalytic process should be identified by the decrease in *Rct* in the presence of the analyte [43,44], while an increase in *Rct* should be associated to an adsorption process [40,45]. We observed a huge increase in *Rct* for p(Py:IMZ-50) in contrast with p(Py:IMZ-0); this is certainly related to the lack of electroactivity of IMZ, that can hinder the charge-transfer process at the electrode/electrolyte interface, as observed for the electrosynthesized copolymer [31]. In the presence of DEDNPP, there was an increase in the *Rct* values for both samples, indicating an adsorption of DEDNPP molecules at the electrode surface. The DEDNPP

molecules can block the electron and ion transfer processes [40], as deduced from the decreasing current in the CV mentioned above. The increase in *Rct* was more drastic for p(Py:IMZ-50) as compared to p(Py:IMZ-0), due to the high affinity of the IMZ for the organophosphate.

Both samples presented similar *Qdl* values, indicating that the films have similar morphologies. This proposition is supported by the TEM images in Fig. S3, which also show no significant changes in the presence of DEDNPP. The increase in *Qlf* for the IMZ-containing electrode indicates an increase in the load of intercalated ions in the polymeric film; this fact corroborates the highest capacitive current observed in the cyclic voltammogram of this material [31]. This parameter did not change drastically in the presence of DEDNPP.

Although no significant electrocatalytic activity in DEDNPP degradation has been observed for the p(Py:IMZ) copolymers in the present work, the mechanism of the catalysis could be modified by changing the oxidation state of the copolymer. To verify this proposition, a spectroelectrochemical method was used to measure the reaction kinetics at 360 nm during the application of different potentials. The kinetic experiments were carried out *in situ* with the electrochemical cell assembled inside the cuvette as can be seen in Fig. 5 (a), using the modified p(Py:IMZ-50) electrode as WE. Three different potentials were used for the WE: 0.6 V, in which the polymer is entirely oxidized; ocp, which is the equilibrium potential of the material; and -0.4 V, which corresponds to the reduced state of the polymer.

The copolymer structure considered in this work is shown in Fig. 5 (a), which has been proposed based on the Py polymerization mechanism suggested by Diaz *et al.* [46] and in the regioselectivity of the electrophilic substitution at the C-5 position of the IMZ ring [47,48]. In this way, IMZ becomes part of the conjugated system and its

oxidation can lead to the appearance of positive charges both in Py and IMZ unities. Fig. 5 (b) presents the kinetic curves registered for 110 min with the electrodes at the different potentials. All experiments were carried out in triplicates and the results are shown as mean values with standard deviations. The curves were adjusted using the initial rate method and the $k_{obs}$ values are shown in Fig. 5 (c).

The highest $k_{obs}$ for degradation of DEDNPP was obtained at 0.6 V; this behavior could be explained by the formation of positive charges in PPy during the oxidation. These charges can lead to a rearrangement of the IMZ structure and to the appearance of a positive delocalized charge in the ring, which can cause a modification in the dephosphorylation reaction mechanism. In this case, some of the imidazolium cations can help to activate the OP through interaction of the acidic hydrogen on C-2 with the P=O bonds, while other imidazole moieties can act as nucleophiles through the amine groups (Fig. 5 (d)). This behavior was observed earlier in the catalysis of dephosphorylation using ionic liquids [49].

In the ocp condition, the $k_{obs}$ for p(Py:IMZ-50) was similar to the value obtained in the conventional chemical catalysis since this is the equilibrium potential of the material (the same of the as-synthesized copolymer). For p(Py:IMZ-50), the ocp was 0.0 V and in this condition the copolymer is partially oxidized, as can be seen in the voltammogram in Fig. 4 (b). After applying -0.4 V, we observed a decrease in the $k_{app}$ value that is compatible with the presence of the reduced form of the copolymer at this potential. The absence of imidazolium cations prevents the activation of the substrate, and the catalysis then occurs only by nucleophilic attack at the P=O bonds.

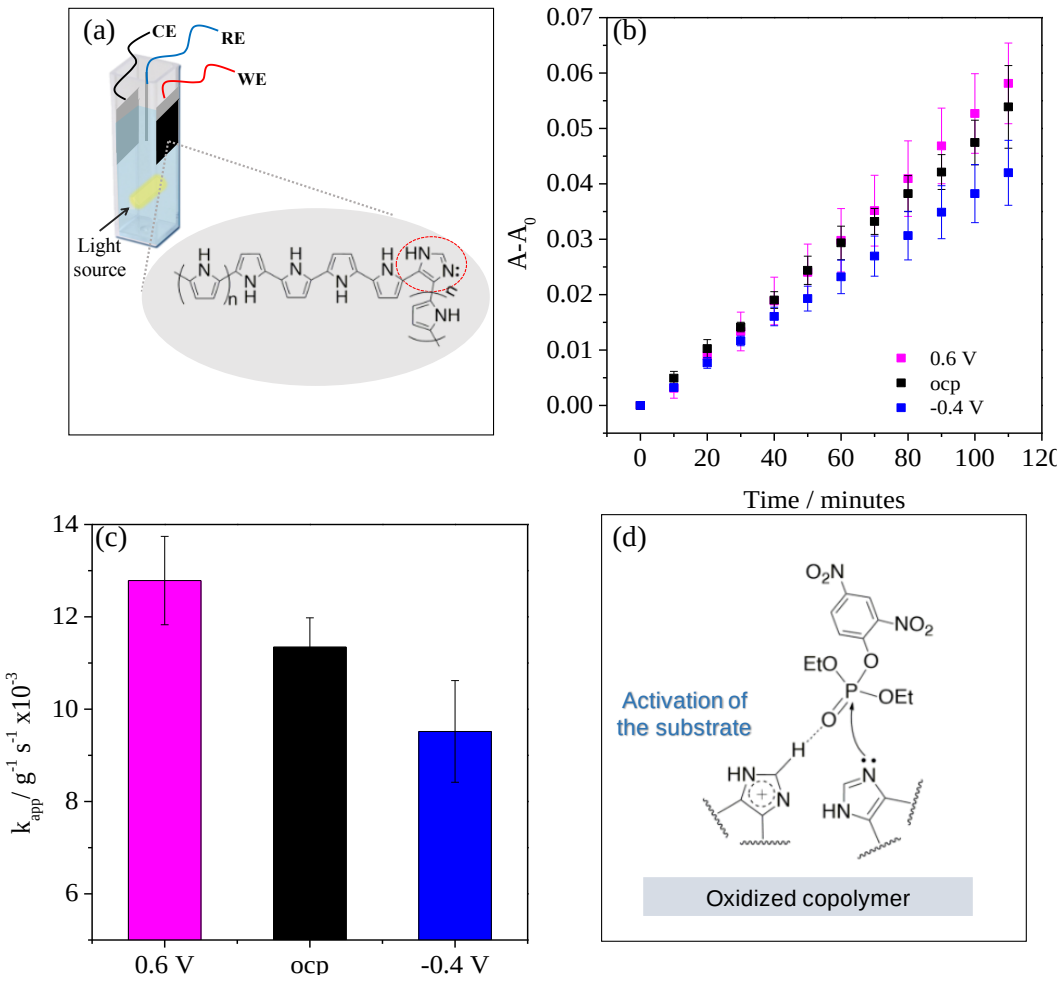


Fig. 5. (a) Schematic representation of the spectroelectrochemical setup using p(Py:IMZ-50) as working electrode (WE), together with the proposed chemical structure for the copolymer. (b) Kinetic curves for p(Py:IMZ-50) during the catalysis of DEDNPP degradation at different potentials and (c) $k_{obs}$ values obtained by fitting the kinetic curves. (d) Mechanism of substrate activation and nucleophilic attack on DEDNPP by the oxidized copolymer.

Overall, our results show that copolymers based on Py and IMZ are efficient for OP degradation as monitored using DEDNPP, and this reaction is potential-dependent, although electrocatalysis does not occur. Based on previous works employing ionic liquids, we propose the mechanism shown in Fig. 5 (d), which suggests that the

oxidized conducting polymer enhances the rate constant of the degradation by a combination of substrate activation and nucleophilic attack at the P=O group.

## 4. Conclusions

Organophosphate compounds present high toxicity to living organisms and high tendency to bioaccumulation, making the development of new degradation catalysts and the understanding of their working mechanisms a subject of pressing concern and interest in the scientific community. Despite the fact that a number of catalysts are already under study, designing a single material with an optimal combination of high efficiency, easy recovery and stimulus responsiveness is a difficult task. In this context, we have developed and applied new copolymers based on pyrrole and imidazole as heterogeneous catalysts for dephosphorylation reaction; our results demonstrate that copolymers with higher IMZ contents presented better catalytic activity. Although rate constants were of the same order of magnitude as those reported for some homogenous catalysts, the facility of recovery and reuse of the heterogeneous systems are advantageous for effective applications. Furthermore, in this work, we have been able to show that polypyrrole does not only act as a matrix to anchor imidazole molecules, but its electroactivity also affects the reaction mechanism as shown by spectroelectrochemical evidence from potential-mediated dephosphorylation. The present study shows new possibilities to combine the good catalytic activity of imidazole and the well-known electroactivity of polypyrrole, leading to a cooperative effect in organophosphate degradation that is certainly important to improve food and environmental safety.

**References:**


[1] P. Pavez, D. Milla, J.I. Morales, E.A. Castro, C. Lo, J.G. Santos, Mechanisms of Degradation of Paraoxon in Different Ionic Liquids, J. Org. Chem. 78 (2013) 9670–9676. doi:10.1021/jo401351v.

[2] M.B. Abou-donia, Organophosphorus Ester-Induced Chronic Neurotoxicity, Arch. Environ. Heal. 58 (2003) 484–497. doi:10.3200/AEOH.58.8.484-497.

[3] C.P. Holstege, M. Kirk, F.R. Sidell, CHEMICAL WARFARE: Nerve Agent Poisoning, Med. Toxicol. 13 (1997) 923–942. doi:0749-0704/97.

[4] R.T. Delfino, T.S. Ribeiro, J.D. Figueroa-villar, Organophosphorus Compounds as Chemical Warfare Agents: a Review, J. Braz. Chem. Soc. 20 (2009) 407–428. doi:10.1590/S0103-50532009000300003.

[5] K. Kim, O.G. Tsay, D.A. Atwood, D.G. Churchill, Destruction and Detection of Chemical Warfare Agents, Chem. Rev. 111 (2011) 5345–5403. doi:10.1021/cr100193y.

[6] I. Mangas, E. Vilanova, Neurotoxic Effects Associated with Current Uses of Organophosphorus Compounds, J. Braz. Chem. Soc. 27 (2016) 809–825. doi:10.5935/0103-5053.20160084.

[7] N. Kaur, N. Prabhakar, Current scenario in organophosphates detection using electrochemical biosensors, Trends Anal. Chem. 92 (2017) 62–85. doi:10.1016/j.trac.2017.04.012.

[8] N. Alvarenga, W.G. Birolli, E.B. Meira, S.C.O. Lucas, I.L. De Matos, M.

Nitschke, L.P.C. Romão, A.L.M. Porto, Biotransformation and biodegradation of methyl parathion by Brazilian bacterial strains isolated from mangrove peat, Biocatal. Agric. Biotechnol. 13 (2018) 319–326. doi:10.1016/j.bcab.2017.12.015.

[9] S.A. Willison, D.S.I. I, A. Mysz, J. Starr, D. Tabor, B. Wyrzykowska-ceradini, J. Nardin, E. Morris, E. Gibb, The impact of wipe sampling variables on method performance associated with indoor pesticide misuse and highly contaminated areas, Sci. Total Environ. 655 (2019) 539–546. doi:10.1016/j.scitotenv.2018.11.128.

[10] R.B. Campos, L.R.A. Menezes, A. Barison, D.J. Tantillo, E.S. Orth, The Importance of Methyl Positioning and Tautomeric Equilibria for Imidazole Nucleophilicity, 4 (2016) 15521–15528. doi:10.1002/chem.201602573.

[11] R. Wang, J. Pan, M. Qin, T. Guo, Molecularly imprinted nanocapsule mimicking phosphotriesterase for the catalytic hydrolysis of organophosphorus pesticides, Eur. Polym. J. 110 (2019) 1–8. doi:10.1016/j.eurpolymj.2018.10.045.

[12] L. Hostert, S.F. Blaskievicz, J.E.S. Fonsaca, S.H. Domingues, A.J.G. Zarbin, E.S. Orth, Imidazole-derived graphene nanocatalysts for organophosphate destruction : Powder and thin film heterogeneous reactions, J. Catal. 356 (2017) 75–84. doi:10.1016/j.jcat.2017.10.008.

[13] C.M. Rufo, Y.S. Moroz, O. V Makhlynets, I. V Korendovych, Copper-Containing Catalytic Amyloids Promote Phosphoester Hydrolysis and Tandem Reactions, (2018) 8–11. doi:10.1021/acscatal.7b03323.

[14] E.S. Orth, T.G. Almeida, V.B. Silva, A.R.M. Oliveira, F. Maria, M. Ocampos, A. Barison, Mechanistic insight on the catalytic detoxification of Paraoxon mediated by imidazole: Furnishing optimum scaffolds for scavenging organophosphorus

agents, J. Mol. Catal. A Chem. 403 (2015) 93–98. doi:10.1016/j.molcata.2015.03.020.

[15] K.L. Klinkel, L.A. Kiemele, D.L. Gin, J.R. Hagadorn, Effect of ligand modifications and varying metal-to-ligand ratio on the catalyzed hydrolysis of phosphorus triesters by bimetallic tetrabenzimidazole complexes, 267 (2007) 173–180. doi:10.1016/j.molcata.2006.11.032.

[16] J. Kla, P. Kla, J. Weber, R. Kurkova, Photolytic degradation of methyl-parathion and fenitrothion in ice and water : Implications for cold environments, Environ. Pollut. 157 (2009) 3308–3313. doi:10.1016/j.envpol.2009.05.045.

[17] C. Wu, K.G. Linden, Degradation and byproduct formation of parathion in aqueous solutions by UV and UV/H2O2treatment, Water Res. 42 (2008) 4780–4790. doi:10.1016/j.watres.2008.08.023.

[18] P.V. Laxma, K. Kim, A review of photochemical approaches for the treatment of a wide range of pesticides, J. Hazard. Mater. 285 (2015) 325–335. doi:10.1016/j.jhazmat.2014.11.036.

[19] R.K. Sit, V. V Fokin, G. Amitai, K.B. Sharpless, P. Taylor, Z. Radic, Imidazole Aldoximes Effective in Assisting Butyrylcholinesterase Catalysis of Organophosphate Detoxification, J. Med. Chem. 57 (2014) 1378–1389. doi:10.1021/jm401650z.

[20] P.G. Besant, P. V Attwood, Histidine Phosphorylation in Histones and in Other Mammalian Proteins, 1st ed., Elsevier Inc., 2010. doi:10.1016/S0076-6879(10)71021-1.

[21] P. V Attwood, M.J. Piggott, X.L. Zu, P.G. Besant, Focus on phosphohistidine,

Amino Acids. 32 (2007) 145–156. doi:10.1007/s00726-006-0443-6.

[22] E.S. Orth, E.H. Wanderlind, M. Medeiros, P.S.M. Oliveira, B.G. Vaz, M.N. Eberlin, A.J. Kirby, F. Nome, Phosphorylimidazole Derivatives : Potentially Biosignaling Molecules, J. Org. Chem. 76 (2011) 8003–8008. doi:10.1021/jo2017394.

[23] V.B. Silva, E.S. Orth, Are Imidazoles Versatile or Promiscuous in Reactions With Organophosphates? Are Imidazoles Versatile or Promiscuous in Reactions with Organophosphates? Insights From the Case of Parathion, J. Braz. Chem. Soc. 00 (2019) 1–11. doi:10.21577/0103-5053.20190084.

[24] H. Kitano, Z. Sun, N. Ise, Functionalized Polymer Latices. 2. Catalytic Effects of Imidazole-Containing Latices on Hydrolyses of Phenyl Esters, Macromolecules. 16 (1983) 1306–1310. doi:10.1021/ma00242a010.

[25] G.L. Ferreira, A. Grein-iankovski, M.A.S. Oliveira, F.F. Simas-tosin, I.C. Riegel-vidotti, E.S. Orth, A tailored biocatalyst achieved by the rational anchoring of imidazole groups on a natural polymer : furnishing a potential artificial nuclease by sustainable materials engineering, ChemComm. 51 (2015) 6210–6213. doi:10.1039/c5cc00860c.

[26] S. Wang, L. Bromberg, H. Schreuder-gibson, T.A. Hatton, Organophophorous Ester Degradation by Chromium(III) Terephthalate Metal − Organic Framework (MIL-101) Chelated to N , N - Dimethylaminopyridine and Related Aminopyridines, ACS Appl. Mater. Interfaces. 5 (2013) 1269–1278. doi:10.1021/am302359b.

[27] P. Innocenzi, D. Carboni, L. Malfatti, A. Pinna, B. Lasio, Molecularly imprinted La-doped mesoporous titania films with hydrolytic properties toward

organophosphate pesticides, New J. Chem. 37 (2013) 2995–3002. doi:10.1039/c3nj00291h.

[28] F. Wolfart, B.M. Hryniewicz, L.F. Marchesi, E.S. Orth, D.P. Dubal, P. Gómez-Romero, M. Vidotti, Direct electrodeposition of imidazole modified poly(pyrrole) copolymers: synthesis, characterization and supercapacitive properties, Electrochim. Acta. 243 (2017). doi:10.1016/j.electacta.2017.05.082.

[29] D.Y. Kim, J.Y. Lee, D.K. Moon, C.Y. Kim, Stability of Reduced Polypyrrole, Synth. Met. 69 (1995). doi:10.1016/0379-6779(94)02531-3.

[30] J. Huang, C. Chu, Achieving efficient poly (3, 4-ethylenedioxythiophene)-based supercapacitors by controlling the polymerization kinetics, Electrochim. Acta. 56 (2011) 7228–7234. doi:10.1016/j.electacta.2011.03.044.

[31] F. Wolfart, B.M. Hryniewicz, L.F. Marchesi, E.S. Orth, D.P. Dubal, P. Gómez-romero, M. Vidotti, Direct electrodeposition of imidazole modified poly(pyrrole) copolymers: synthesis, characterization and supercapacitive properties, Electrochim. Acta. 243 (2017) 260–269. doi:10.1016/j.electacta.2017.05.082.

[32] N. Su, H.B. Li, S.J. Yuan, S.P. Yi, E.Q. Yin, Synthesis and characterization of polypyrrole doped with anionic spherical polyelectrolyte brushes, EXPRESS Polym. Lett. 6 (2012) 697–705. doi:10.3144/expresspolymlett.2012.75.

[33] L. Ruangchuay, J. Schwank, A. Sirivat, Surface degradation of a-naphthalene sulfonate-doped polypyrrole during XPS characterization, Appl. Surf. Sci. 199 (2002) 128–137. doi:10.1016/S0169-4332(02)00564-0.

[34] C. Malitesta, I. Losito, L. Sabbatini, P.G. Zambonin, Applicability of chemical derivatization – X-ray photoelectron spectroscopy (CD–XPS) to the

characterization of complex matrices: case of electrosynthesized polypyrroles, J. Electron Spectrosc. 97 (1998) 199–208. doi:10.1016/S0368-2048(98)00298-9.

[35] L. Wan, X. Wang, S. Wang, S. Li, Q. Li, R. Tian, M. Li, Synthesis, characterization, and electrochemical properties of imidazole derivatives functionalized single-walled carbon nanotubes, J. Physycal Org. Chem. 22 (2009) 331–336. doi:10.1002/poc.1481.

[36] L. Stroea, T. Buruiana, E.C. Buruiana, Synthesis and solution properties of thermosensitive hydrophilic imidazole- based copolymers with improved catalytic activity, Mater. Chem. Phys. 223 (2019) 311–318. doi:10.1016/j.matchemphys.2018.10.066.

[37] M. Fuensanta, A. Grau, M.D. Romero-Sánchez, C. Guillem, Á.M. López-Buendía, Effect of the polymer shell in imidazole microencapsulation by solvent evaporation method, Polym. Bull. 70 (2013) 3055–3074. doi:10.1007/s00289-013-1007-z.

[38] J.G.L. Ferreira, E.S. Orth, Degrading Pesticides with Waste Product: Imidazole-Functionalized Rice Husk Catalyst for Organophosphate Detoxification, 28 (2017) 1760–1767.

[39] L. Hostert, R.B. Campos, J.E.S. Fonsaca, V.B. Silva, S.F. Blaskievicz, J.G.L. Ferreira, W. Takarada, N. Naidek, Y.H. Santos, L.L.Q. Nascimento, A.J.G. Zarbin, E.S. Orth, Targeted catalytic degradation of organophosphates : pursuing sensors, Pure Appl. Chem. (2018).

[40] H.-C. Wang, H. Zhou, B. Chen, P.M. Mendes, J.S. Fossey, T.D. James, Y. Long, A bis-boronic acid modified electrode for the sensitive and selective determination of glucose concentrations, Analyst. 138 (2013) 7146–7151.

doi:10.1039/c3an01234d.

[41] F. Wolfart, B.M. Hryniewicz, M.S. Góes, C.M. Corrêa, R. Torresi, M.A.O.S. Minadeo, S.I. Córdoba de Torresi, R.D. Oliveira, L.F. Marchesi, M. Vidotti, Conducting polymers revisited: applications in energy, electrochromism and molecular recognition, J. Solid State Electrochem. 21 (2017). doi:10.1007/s10008-017-3556-9.

[42] L.F. Marchesi, S.C. Jacumasso, R.C. Quintanilha, H. Winnischofer, M. Vidotti, The electrochemical impedance spectroscopy behavior of poly(aniline) nanocomposite electrodes modified by Layer-by-Layer deposition, Electrochim. Acta. 174 (2015) 864–870. doi:10.1016/j.electacta.2015.05.077.

[43] B.M. Hryniewicz, M. Vidotti, PEDOT Nanotubes Electrochemically Synthesized on Flexible Substrates: Enhancement of Supercapacitive and Electrocatalytic Properties, ACS Appl. Nano Mater. 1 (2018) 3913–3924. doi:10.1021/acsanm.8b00694.

[44] A.J.S. Ahammad, A. Al Mamun, T. Akter, M.A. Mamun, S. Faraezi, F.Z. Monira, Enzyme-free impedimetric glucose sensor based on gold nanoparticles / polyaniline composite film, J. Solid State Electrochem. 20 (2016) 1933–1939. doi:10.1007/s10008-016-3199-2.

[45] S.L. Jordana, M.D.L. Oliveira, C.P. De Melo, C.A.S. Andrade, Impedimetric sensor of bacterial toxins based on mixed (Concanavalin A)/polyaniline films, Colloids Surfaces B Biointerfaces. 117 (2014) 549–554. doi:10.1016/j.colsurfb.2013.12.057.

[46] E.M. Genies, G. Bidan, A.F. Diaz, Spectroelectrochemical Study of Polypyrrole Films, 149 (1983) 101–113. doi:10.1016/S0022-0728(83)80561-0.

[47] S. Narayanan, S. Vangapandu, R. Jain, Regiospecific Synthesis of 2,3-Disubstituted-L-Histidines and Histamines, Bioorg. Med. Chem. Lett. 11 (2001) 1133–1136. doi:10.1016/S0960-894X(01)00154-8.

[48] F. Aldabbagh, W.R. Bowman, E. Mann, A.M.Z. Slawin, Bu3SnH Mediated Oxidative Radical Cyclisation onto Imidazoles and Pyrroles Fawaz, Tetrahedron. 55 (1999) 8111–8128. doi:10.1016/S0040-4020(99)00419-6.

[49] J.G.L. Ferreira, L.M. Ramos, A.L. De Oliveira, E.S. Orth, B.A.D. Neto, An Ionically Tagged Water-Soluble Artificial Enzyme Promotes the Dephosphorylation Reaction with Nitroimidazole: Enhanced Ionic Liquid E ff ect and Mechanism, J. Org. Chem. 80 (2015) 5979–5983. doi:10.1021/acs.joc.5b00750.